Combining X-ray CT and DIC to understand the bending strength of OSB

Wanzhao Li[1,2], Donghu Li[2], Yanjun Duan[4], Changtong Mei[1,2],

Jan Van den Bulcke[3], Joris Van Acker[2,3]

[1]Co-
Innovation Center of Efficient Processing and Utilization of Forest Resources, Nanjing Forestry University,
Longpan Road 159, 210037 Nanjing , China

[2]College of Materials Science and Engineering, Nanjing Forestry University, Longpan Road 159, 210037 Nanjing, China

[3]UGent-Woodlab, Laboratory of Wood Technology, Department of Environment, Faculty of Bioscience Engineering, Ghent University, Coupure Links 653, 9000 Ghent, Belgium

[4]National Engineering Research Center of Biomaterials, Nanjing Forestry University, Nanjing, Jiangsu, China

Abstract:

Oriented strand board (OSB) is an important engineered wood product manufactured through bonding of wood strands in cross-oriented layers. The bending strength, one of the crucial properties for loadbearing material, of OSB strongly depends on its structural characteristics. To understand the bending strength of OSB, strain distribution was continuously monitored during a three-point bending test using digital image correlation (DIC) and internal structure was recorded before and after bending using X-ray computed tomography (X-ray CT) respectively. Specimens were cut either along the length (L specimens) or width (W specimens) of OSB panels. For all specimens, strain accumulation mainly seemed to occur in the top and bottom layers and then propagate along or across the central layer. Structural changes in the top and bottom layers of L specimens was either strand delamination or snap off, while only snap off is found in W specimens. This is the main reason of high modulus of elasticity (MOE) and modulus of rupture (MOR) of L specimens in comparison to W specimens. High MOR of the specimens is attributed to strain propagation along the central layer, which can absorb energy from loading. Strain propagation across the central layer causes low MOR, resulting from failure of small strands and delamination in the central layer. Different modes of structural change lead to large variability of MOE, MOR and deformation of the specimens even cut from a single OSB panel. Understanding the bending strength contributes to optimizing the production and application of OSB.

Keywords: *Oriented strand board; Bending strength; Strain distribution; Internal structure*

1. Introduction

Oriented strand board (OSB) is an environmental- and economic-friendly material made from mainly fresh wood, both from small and large diameter logs. OSB is composed of cross-oriented layers consisting of thin and rectangular wooden flakes or strands that are compressed

and bonded together with synthetic resin adhesives. Its cross layered structure is similar with plywood and OSB is widely applied as soleplate of shipping container, wall sheath in building, base plate of floor and so on [1,2]. To applying OSB in more filed as a loadbearing material, its mechanical performance still needs to be improved, for example: increasing it strength and homogenizing the mechanical properties is needed. The mechanical performances of OSB is closely related to its internal structure. Dai et al. found that the bending strength of OSB was influenced by the vertical density profile (VDP) [3,4]. The modulus of elasticity (MOE) of OSB can be increased by optimizing VDP. The effect of VDP on MOE is more serious in high density than in low density OSB. Strands' shape, wood species, direction of alignment of strands and resin distribution all have an impact on the mechanical performance of OSB [5,6]. Randomly distributed voids between strands can deform, resulting in initiation and propagation of cracks in OSB as performing loading tests [7]. As a bio-based material, the mechanical strength of OSB is prone to be affected by environmental conditions as well, such as relative humidity and temperature. Moisture adsorption causes an increase in thickness and softens strands, resulting in a decrease in the bending strength of OSB under cyclic fatigue testing [8,9]. In addition to investigate the factors influencing the mechanical performance of OSB, understanding the dynamic processes of mechanical failure is certainly an interesting research topic. In situ tracking the strain shift and revealing the structural changes is needed to understand the mechanical performance of OSB. These ideas have been successfully applied in investigating the mechanical performance of wood and cross laminated timber [10,11]. Understanding the mechanisms of mechanical failure can scientifically guide production strategies of OSB. It is therefore possible and necessary to investigate the mechanical performances of OSB with a dynamic and holistic view.

Digital image correlation (DIC) is a proven technique for dynamically recording the strain distribution in wood-based composites [12]. This technique quantifies surface deformation of a material by analyzing series of photographs recorded by synchronized cameras. An algorithm then solves the deformations in the collected photographs [13]. X-ray computed tomography (CT) has been extensively used to visualize the internal structure of wood based composites [14,15]. Since the grey scale value of CT data linearly relates to density, a density variation of the wood-based materials could be deduced with X-ray CT [16,17]. Combining DIC and X-ray CT is able to dynamically map the strain distribution and internal structural changes, which is certainly helpful for understanding the mechanical performance of OSB.

The objective of this study is to understand the mechanisms of mechanical failure induced by bending test, because bending strength is a crucial parameter for OSB aiming as a loadbearing material in package, floor and building field. This study uses a holistic view to investigate the bending strength of small amount of specimens. In International standard (ISO16894), bending strength, along panels' length and width respectively, is a key reference to classify OSB [18]. The bending strength of OSB was determined using a three-point bending test, and strain distribution was monitored simultaneously using DIC. Before and after

performing the bending test, the internal structure of the specimens was recorded using X-ray CT. Bending strength of OSB was analyzed by tracking strain distribution shift and revealing the failure features. Modulus of rupture (MOR) and MOE of the specimens could be understood. By relating the failure mechanisms to bending strength, it is going to be possible to optimize the producing and applying technologies of OSB.

2. Material and Methods

2.1 Preparation of specimens

One type of commercially available three-layered OSB panels, produced by Norbord, was used in this experiment. The panels were produced with poplar (*Populus euramericana*) strands, glued by diphenylmethane diisocyanate (MDI). The panels were intended to be used for structural bearing purposes in dry conditions, and were classified as OSB-2 type according to ISO16894 [18]. The density and thickness of the panels were 594.4±32.5kg/m^3 and 15.0mm respectively. OSB has three layers that are named as top, central and bottom layer, and their average thicknesses were approximately 2.5mm, 10.0mm and 2.5mm respectively. These values were measured after conditioning nine representative specimens, with cross sections of 50×50 mm^2, at 65±5% relative humidity (RH) and 20±1°C for four weeks. Afterwards, nine specimens with cross sections of 260×40 mm^2 were cut along length and width directions of OSB panels respectively. In OSB standard, bending strength in both length and width directions of panels needs to be higher than specific requirements. Specimens cut along panels' length and width direction were so called L and W specimens (Fig.1). The middle region at one side of three L specimens and three W specimens was slightly polished using sand paper, before speckle patterns were created in the region of interest (ROI) by manually dotting the surface with a black gel pen (Fig.2). Thereafter, these specimens were scanned with X-ray computed tomography (X-ray CT), mechanically tested using three-point bending (3P) and then re-scanned with X-ray CT. For six L specimens and six W specimens without speckle patterns, they were only measured using 3P test.

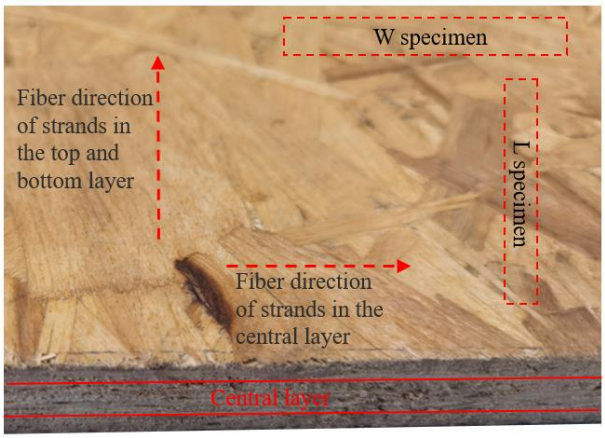

Fig.1. Illustration of OSB and the specimen's preparation.

2.2 X-ray CT scanning

The specimens with speckle patterns were scanned with the X-ray CT scanner (Sanying Precision Instruments Corporation, EFPscan-2000) installed at Nanjing Forestry University. This device can scan the specimens with the maximum length of 300mm. The internal structure regarding to ROI of the specimens, therefore, was recorded. A single spiral scan was optimized to complete in 70 min, and a voxel pitch of approximately 36μm was obtained. 1080 projections were acquired at a tube voltage of 145kV, current of 85μA, 0.5s exposure, and no filter. All tomographic reconstructions were performed (iteration number of 2) using the software package Voxel Studio Reconstruction.

2.3 Bending test and digital image correlation

The bending strength of OSB specimens was measured with a 3P test using a universal testing machine (Instron 5966, USA). This device can record the displacement of the loading wedge (±0.001mm), and the loading force (±0.001N), at 10Hz. The distance between the two supports was 210mm. The velocity of the loading wedge was set at 5mm/min. The displacement of the loading wedge was regarded to be the specimens' deformation. Considering the high density and stiffness in the top layer of OSB, indentation induced with loading wedge was believed to be small. For the specimens with speckle patterns, throughout the bending test, the strain distribution in the ROI was computed with DIC. The image correlation was performed using the commercial software package Correlated Solutions (www.correlatedsolutions.com). Photographs were captured every 0.2s by a CCD camera. The distance between the camera and specimen was approximately 200mm. To increase the signal-to-noise ratio the speckle patterns were illuminated by a Lowel Pro LED light. The specimens were positioned in the Instron universal testing machine, and image capture and loading if the specimen were then started simultaneously. Thus, each picture represents a distinct loading stage (Fig.2). There were 50 pixels/mm^2.

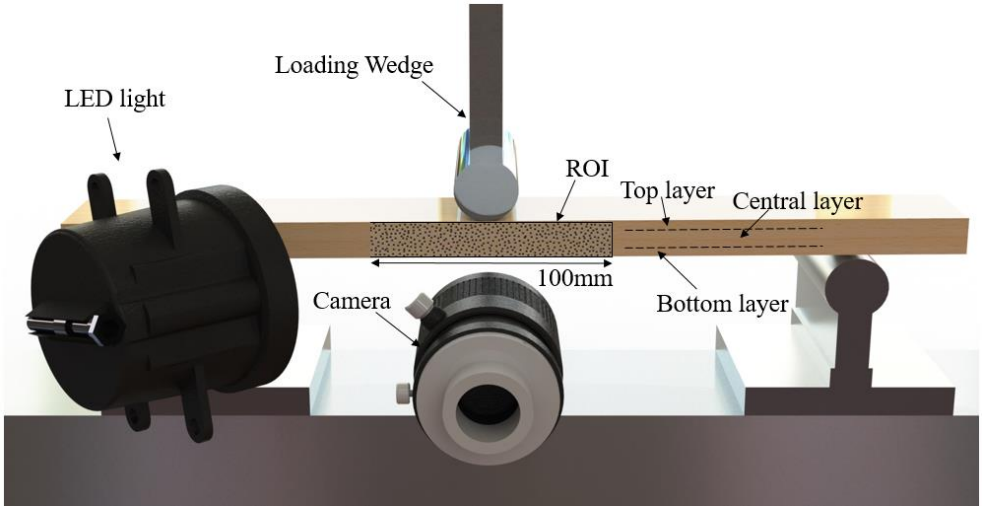

Fig.2. Illustration of the test set-up.

2.4 Data processing

Strain distributions were acquired with DIC, using the Lagrange Tensor. Bending strain was determined along the panel thickness direction, positive and negative values indicate tension and compression respectively. For shear strain, positive values indicate clockwise shear and negative values indicate anti-clockwise shear. To obtain strain propagation, dynamic strain distribution was tracked in function of 5 load steps. Considering the different failure load in terms of the specimens, different interval between two load steps was used in analyzing data. The interval between two load steps was determined based on the failure load of a specimen. Specifically, the load step interval was set to be 0.2 times of the failure load of a specimen. In order to track the strain shift, strain changes in each pixel were calculated. Strain obtained in different steps was compared in terms of the position of pixels. Specifically, the pixels' position from two steps were matched in ahead and then strain changes in a pixel with the same position was calculated using Matlab. For instance, strain changes from 0.8 to 1.0 times of the failure load could be calculated according to Eq.1 and Eq.2. In this study, strain changes from 0.4 to 0.6, from 0.6 to 0.8, and from 0.8 to 1.0 times of the failure load were analyzed.

$$SC_b=S_{b\text{-}1}-S_{b\text{-}0.8} \quad (1)$$

$$SC_s=S_{s\text{-}1}-S_{s\text{-}0.8} \quad (2)$$

with SC_b: the bending strain change in a pixel, $S_{b\text{-}1}$: the bending strain in a pixel at 1.0 times of the failure load, $S_{b\text{-}0.8}$: the bending strain in a pixel at 0.8 times of the failure load, SC_s: the shear strain change in a pixel, $S_{s\text{-}1}$: the shear strain in a pixel at 1.0 times of the failure load, $S_{b\text{-}0.8}$: the shear strain in a pixel at 0.8 times of the failure load.

3. Results and discussion

3.1 Mechanical properties

Fig.3 presents the modulus of rupture (MOR), modulus of elasticity (MOE) and displacement of loading wedge (regarding as deformation of the specimens). There is clear variability in both bending strength and displacement, although all the specimens are cut from a single OSB panel. In comparison to MOE, the variability of MOR is large. MOR and MOE in specimens cut along panels' length direction (L specimens) are much higher than those in specimens cut along panels' width direction (W specimens). This is because of the cross layered structure of OSB and high tensile strength of wood in the fiber direction [9]. Despite of the lower MOR and MOE, deformation in W specimens is larger. Higher MOR means more energy consumption during the failure of the specimens. Energy consumption positively relates to specimens' stiffness and deformation [19].

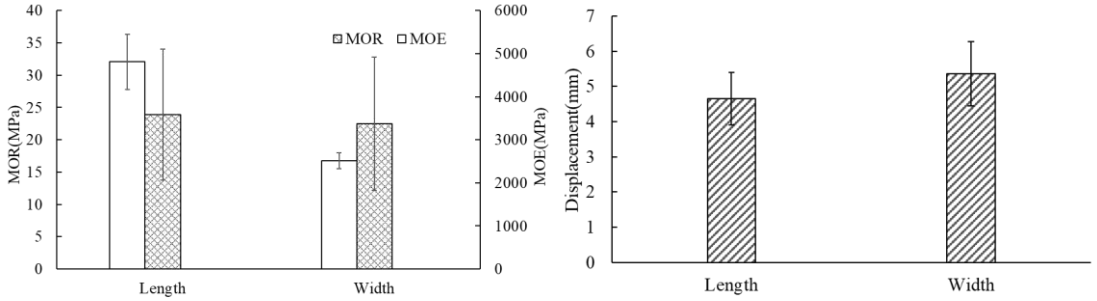

Fig.3. MOR, MOE and deformation of nine specimens cut along panels' length and width directions respectively.

In order to further understand the bending strength of OSB, six specimens with speckle patterns are investigated in detail. Their MOR, MOE and displacement are listed in Table 1. Although MOE of L-1 is higher than L-2, MOR of L-2 is higher than L-1. MOE of W-1 is slightly higher than both W-2 and W-3, however, MOR of W-1 is the lowest of the three specimens. MOR linearly relates to specimens' failure load, however, MOE is mainly determined with the slope of load and displacement curve. Fig.4 shows the relationship between loading force and displacement (specimens' deformation). For wood-based materials, the deformation mainly consists of elastic and plastic deformation. Two sections of deformation are obvious in L-2 and the deflection point is highlighted with arrow. These two sections closely relate to elastic and plastic deformation. The second part of section (plastic deformation), however, is non-obvious in L-1 and L-3. Plastic deformation in W-2 and W-3 is more obvious than that in W-1. Large plastic deformation means high failure load and MOR. The modes of deformation are determined with the strain transferal and internal structural changes.

Table 1

MOE, MOR and displacement of six specimens with speckle patterns.

Properties	L-1	L-2	L-3	W-1	W-2	W-3
MOR(MPa)	23.6	29.1	18.1	8.4	17.8	22.7
MOE(MPa)	4854.2	4239.4	3638.7	2596.4	2534.9	2562.6
Displacement(mm)	3.5	5.7	3.8	4.7	7.3	6.4

Note: L and W indicate the specimens cut along panels' length and width direction respectively.

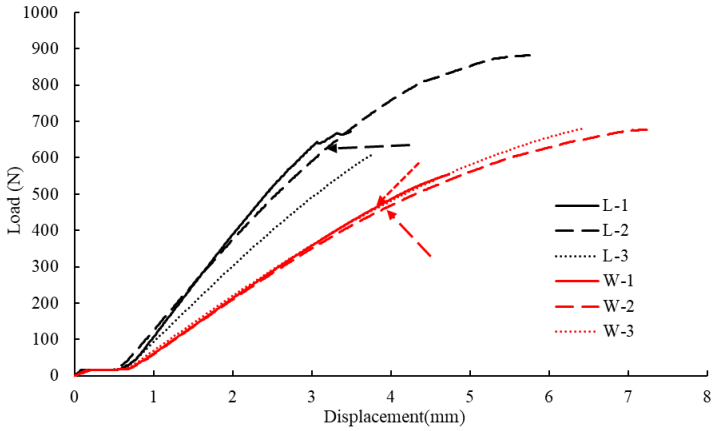

Fig.4. The relationship between loading force and displacement of six specimens with speckle patterns. Deflection of elastic and plastic deformation is highlighted with arrows.

3.2 Dynamic strain transferal

Fig.5and Fig.6 show the strain distribution changes of six specimens at three steps, namely 60%, 80% and 100% of the failure load. Strain distribution changes at 60%, 80% and 100% are strain changes from 0.4 to 0.6, from 0.6 to 0.8, and from 0.8 to 1.0 times of the failure load. Generally speaking, strain distribution changes in L specimens is more significant than in W specimens. For L specimens, strain is prone to transfer from top and bottom layers to central layer. For W specimens, strain accumulation in top and bottom layer is obvious. Local strain enlargement is more obvious than inter-layer strain transferal.

Both shear and bending strain in L-2 is larger than in L-1 and L-3 (Fig.5). It agrees with that fact that displacement in L-2 is larger than in L-1 and L-3 (Fig.4). The strain area in L-2 is also larger than in L-1 and L-3. Effective strain transferal means large energy consumption and high MOR. The maximum energy consumption, however, has little influence on MOE. Taking a close look at L-3, small strains accumulate in the bottom layer and are hardly transferred to other regions. This could be due to the occurrence of structural ruptures at a low loading force. Although strains accumulation do seem moderate, the specimen still fails. As such, both MOR and MOE of L-3 are unsurprisingly low. For L-1, the stiffness of top and bottom layers is high, which contributes to a high MOE. Strain transferal along the central layer of L-1 is not substantial, resulting in small energy consumption and a low MOR.

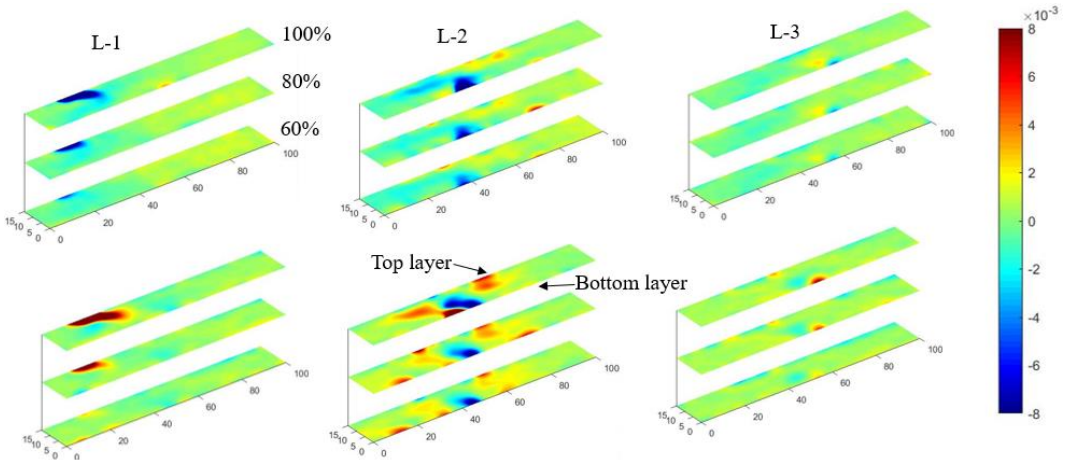

Fig.5. Shear strain (first row) and bending strain (second row) at three steps (60%, 80% and 100% of the failure load) in three specimens cut along the length direction of the panels. Note: the length and thickness of the ROI are 100mm and 13mm respectively.

Fig.6 shows that both shear and bending strain are prone to accumulate in top and bottom layers of W specimens. Compared to L specimens, strain distribution in the central layer is pronounced in W specimens. These phenomena are caused by the cross layered structure of OSB. On the one hand, strength of wood along the grain direction is much higher than in the tangential direction. On the other hand, flexibility of wood along the grain direction is poor in comparison to tangential direction. Due to these factors, deformation in top and bottom surfaces of W specimens is large at low loading force. Meanwhile, structural ruptures will be less apparent due to greater flexibility in that direction. This hypothesis agrees with the fact of large displacement but low MOR and MOE of W specimens. Taking a close look at W-1, strain mainly accumulates in local regions in top and bottom layers. Strain hardly transfers along top and bottom layers or across the central layer of the specimen. This means only a low amount of energy can be absorbed via strain transferal, resulting in a low MOR.

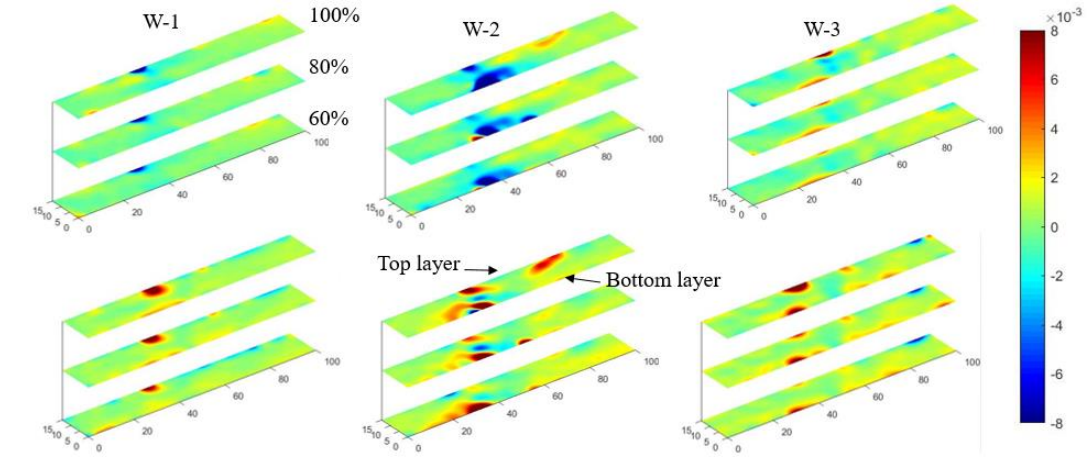

Fig.6. Shear strain (first row) and bending strain (second row) at three steps (60%, 80% and 100% of the failure load) in three specimens cut along the width direction of the panel. Note: the length and thickness of ROI are 100mm and 13mm respectively.

Fig.7 demonstrates the strain distribution at the failure load of six specimens during the 3P test. Shift of strain distribution is also highlighted. For L-1, strain mainly accumulates in the top layer even at 80% of the failure load. Afterwards, strain quickly crosses the central layer. For L-2, obvious strain is found in the central layer at 80% of the failure load. Next, strain transfers along the central layer. Based on the structural characteristics of OSB, both density and stiffness in top and bottom layers is high [7]. As such, it can be assumed that elastic deformation of the specimens is mainly determined by the stiffness of the top and bottom layers. Plastic deformation occurs as soon as there is local structural changes. The lower density and porous structure in the central layer can less effectively transfer stress, resulting in structural changes but without structural failure. These hypotheses are supported by the fact that the deflection point, which is assumed the change from elastic to plastic deformation, of L-2 happens at approximately 60% of the failure load (550N) (Fig.3).

Considering the relatively low stiffness and good flexibility of the top and bottom layers of W specimens, strain is prone to transfer to the central layers at low loading force. As it is well known, large shear stress mainly occurs in the neutral layers of a beam under a 3P test. Grain direction of wood strands in the central layer of W specimens is parallel to the beam length. Meanwhile, shear strength of wood loaded parallel to the grain is low. Large shear strain, therefore, is expected in the central layer.

Based on the above results and analysis, strain accumulation and shift need to be optimized in order to improve the MOR and MOE. At the early loading stage, it is good to accumulate strain in top and bottom layers, resulting in high MOE. At the final loading stage, leading strain transferal along the central layer to elongate plastic deformation and increase MOR. This strain distribution shift strategy could be fulfilled by optimizing wood strands alignment and hot pressing parameters, which is going to be done in next step research work.

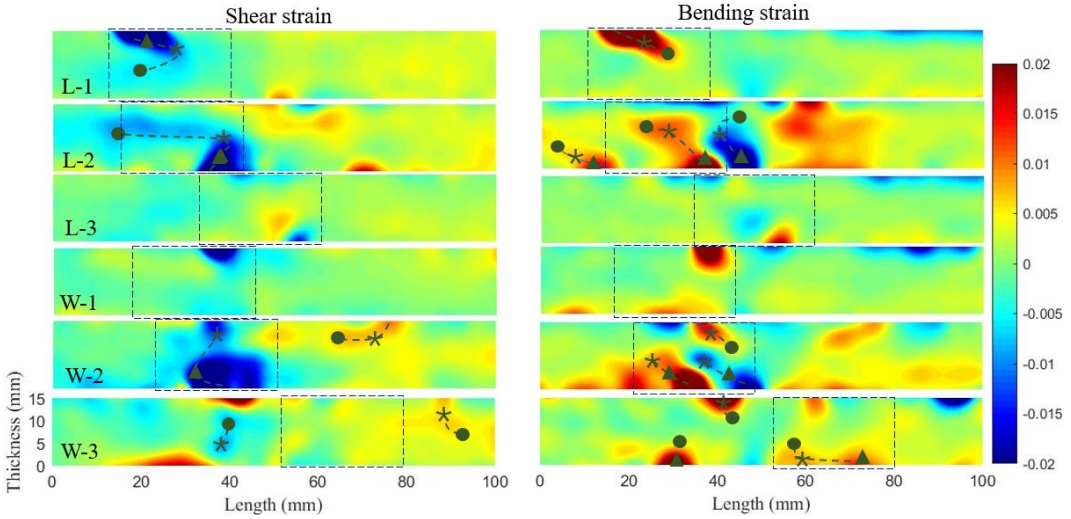

Fig.7. Shear strain and bending strain distribution at failure load in three specimens cut along panels' width direction. The shift in strain distribution is highlighted with dashed lines. Triangle, star and circle patterns indicate 60%, 80% and 100% of the failure load respectively. Dashed squares indicate the regions visualized with X-ray CT in the next section.

3.3 Internal structural changes

Fig.8 and Fig.9 show the internal structure of six specimens before and after 3P test. Strain distribution is caused by internal structural changes, resulting in failure of specimens. In general, obvious internal structural changes are found in regions with serious strain accumulation. Internal structural changes shown in Fig.8 and Fig.9 correspond with locations highlighted with dashed squares in Fig.7. The hypothesis of internal structure evolution, therefore, could be obtained in function of strain shift. Porous structure of the specimens is significantly changed by the bending test. The size and the shape of the voids between wood strands is differentiated by comparing the internal structure of the same location before and after bending test.

The internal structural changes in L-1 mainly occur in the top layer (Fig.8). Specifically, bonded wood strands are delaminated during the early stage of the 3P test. Afterwards, ruptures are induced in strands located beneath areas of delamination. Finally, ruptures propagate across the thickness direction, resulting in failure. This means that the top layer effectively protects the central layer from structural changes. Accumulated structural changes in the top layer and limited structure changes in the central layer lead to high MOE but low MOR. Obvious ruptures are found in the bottom layer of L-2, which propagates to the central layer. Ruptures in the bottom layer are strand delamination and snap off. Taking a closer look at the region of snap off, a loose structure and lack of resin protection are noted. In comparison to snap off, delamination is able to protect the central layer from structural changes. It is found that the internal structure in the central layer of L-2 is changed substantially. These results agree with the findings from other researchers [20,21]. They indicated that energy could be absorbed by internal structural deformation of OSB, resulting from the occurrence of micro-cracks in strands, strand failure, debonding and delamination of the samples under a 3P test. Voids between strands are squeezed or enlarged, but ruptures in wood strands are not obvious in the central layer of L2. By comparing the internal structure of L-3 before and after the 3P test, it is found that ruptures almost only occur in a small region. This region is adjacent to the side face of the specimen. Accumulation of ruptures is due to the low strength locally, which results from local loose structure. Ruptures more or less directly cross the thickness of the specimen. In this case, only limited regions could be buffering zones to consume energy before the specimen fails, which leads to a low MOR of L-3.

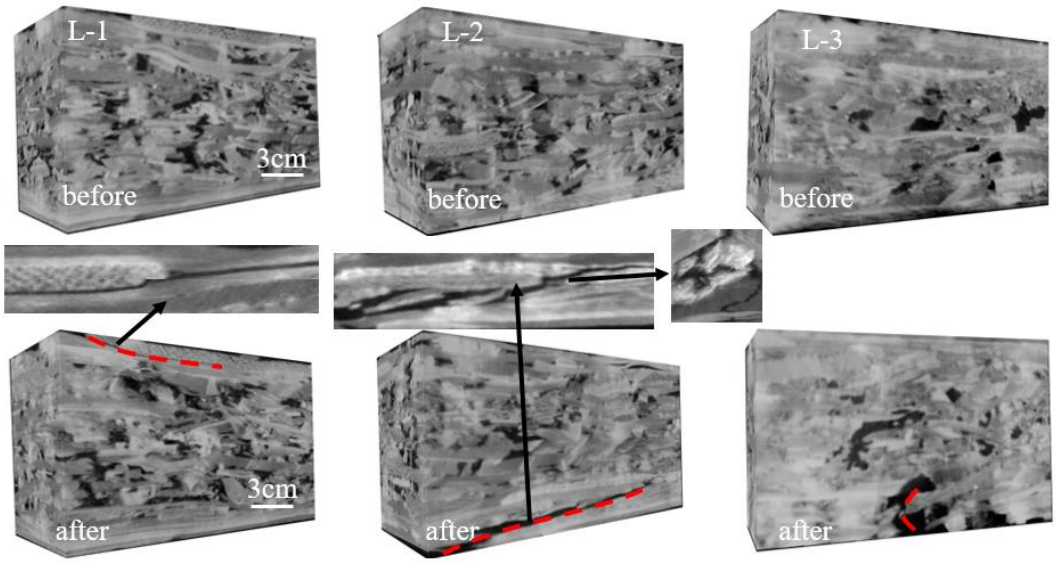

Fig.8. The internal structure of the specimens cut along panel length direction before and after bending test. Red dash lines indicate the ruptures induced with bending test.

Ruptures mainly emerge in the top and bottom layers of W specimens. Ruptures in W specimens are mainly caused by snap off, while there is hardly any strands' delamination (Fig.9). Ruptures emerge in the bottom layer, but there are less visible ruptures in the central layer before failure of the W-1 specimen (Fig.9). Structural changes in the central layer are mainly a reduction in size of the voids between wood strands. This means that the energy absorption by the central layer is small, resulting in a low MOR. Serious structural changes occur in the bottom layer of W-2 and W-3, which is due to a low stiffness and locally loose structure. Ruptures propagate from the bottom layer to the central layer. Internal structural changes in the central layer consist of strand failure and delamination, compression of voids. Strand failure and delamination certainly increase the energy absorption in the central layer and the MOR of W-2 and W-3 specimens (Table 1).

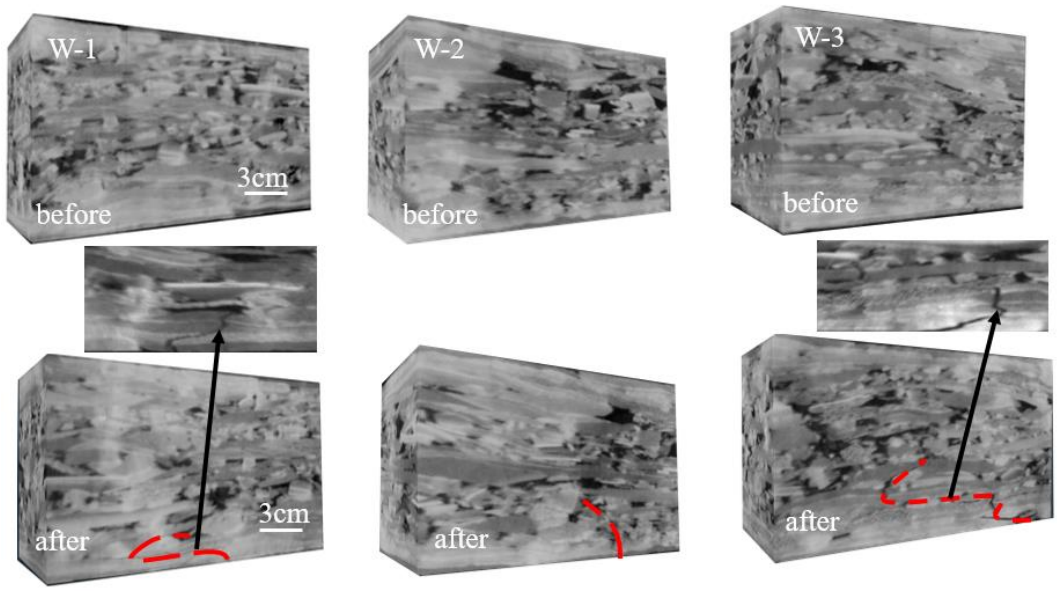

Fig.9. The internal structure of the specimens cut along panel width direction before and after bending test. Red dash lines indicate the ruptures induced with bending test.

In the 3P test, a high density and a homogenized internal structure in top and bottom layers contribute to high stiffness and MOE. Limiting strands snap off is crucial for increasing MOE of both L and W specimens. This could be fulfilled by using well-shaped strands and homogenized resin distribution. The central layer plays an important role in increasing the MOR of both L and W specimens. Large structural changes, such as failure and delamination of strands in the central layer are helpful for absorbing the energy and increasing the MOR. The ruptures are possible to quickly or slowly cross the central layer, which causing large variability of MOR. In order to protect ruptures from quickly crossing the panel thickness, one probably needs to avoid continuous voids along the panel thickness. Limiting the number of small strands could be a strategy. Optimizing the internal structure is going to increase the bending strength and decrease the variability in bending strength. Large bending strength variability seriously limits the application of OSB as a load bearing material. Minimize structural change differences between the specimens certainly is able to decrease bending strength variability.

4. Conclusions

Combining digital image correlation (DIC) with X-ray computed tomography (X-ray CT) is a valuable method to investigate the mechanical performance of OSB. The mechanical performance is studied using a three point bending test. The strain distribution is continuously monitored using DIC, while the changes in internal structure before and after mechanical testing with X-ray CT give valuable insights in the damage patterns. The specimens cut along panels' length direction (L specimens) have a much higher MOE and MOR than the specimens cut along panels' width direction (W specimens). Compared to L specimens, deformation of the W specimens is large. Variability of MOE, MOR and displacement among the same group of specimens is large. For all specimens, strain accumulation is prone to occur in top and bottom

layers and then propagates along or across the central layer. In comparison to directly crossing the central layer, strain propagation along the central layer can increase MOR of the specimens. Different strain distribution modes relate to structural changes. Structural changes in top and bottom layers of L specimens consist of strands' delamination and snap off, while only strand snap off is found in W specimens. Contrary to strand snap off, delamination contributes to a high MOE. Structural changes in the central layer are determined with voids distribution. Generally speaking, structural changes, such as strand failure and delamination in the central layer, result in a large amount of energy absorbed by the material and a high MOR. The findings of this work are helpful for improving the bending strength and decreasing variability of bending strength by optimizing the internal structure of OSB.

DIC is an effective tool to track the dynamic strain distribution, it would be very interesting to study dynamic strain distribution of more duplicates. As such, based on big data base, the relationship between bending strength and strain distribution could be statistically analyzed. The general mechanisms of mechanical failure in 3P test would be obtained. The effect of voids on mechanical performance of OSB still need to be studied in future. This could be conducted on compression test as an initiate.

Acknowledgements

This study was financially supported by National Key R&D Program of China (2021YFD2200602) and the Research Project of Jiangxi Forestry Bureau (NO. 202135). We declare that we have no financial and personal relationships with other people or organizations that can inappropriately influence our work, there is no any commercial or associative interest that represents a conflict of interest in connection with the work submitted.

References:

[1] C. Barbuta, P. Blanchet, A. Cloutier, V. Yadama, E. Lowell, OSB as substrate for engineered wood flooring, European Journal of Wood and Wood Products. 70 (2012) 37-43.

[2] A. Hassanieh, H. Valipour, Experimental and numerical study of OSB sheathed-LVL stud wall with stapled connections, Construction and Building Materials. 233 (2020) 117373.

[3] C. Zhou, C. Dai, G. D. Smith, Modeling vertical density profile formation for strand–based wood composites during hot pressing: Part 1. Model development, Composites, Part B. Engineering. 42B (2011) 1350–1356.

[4] C. Zhou, C. Dai, G. D. Smith, Modeling vertical density profile formation for strand–based wood composites during hot pressing: Part 2. Experimental investigations and model validation, Composites, Part B. Engineering. 42B (2011) 1357–1365.

[5] E. Hamidreza, T. Volker, F. Mehdi, Experimental study on correlation between adhesive penetration pattern and mechanical performances in oriented strand board, European journal of wood and wood products. 79 (2021) 59–74.

[6] B. Zhuang, A. Cloutier, A. Koubaa, Physical and Mechanical Properties of Oriented Strand Board Made from Eastern Canadian Softwood Species, Forests. 13 (2022) 523.

[7] W. Li, C. Chen, J. Shi, C. Mei, P. Kibleur, J. Van Acker, J. Van den Bulcke, Understanding the mechanical performance of OSB in compression tests, Construction and Building Materials. 260 (2020) 119837.1–119837.10.

[8] R. J. H. Thompson, M. P. Ansell, P. W. Bonfield, J. M. Dinwoodie, Fatigue in wood–based panels. Part 2: property changes during fatigue cycling of OSB, chipboard and MDf, Wood science and technology. 39 (2005) 311–325.

[9] W. Li, J. Van den Bulcke, D. Mannes, E. Lehmann, I. De Windt, M. Dierick, J. Van Acker, The effect of water sorption/desorption on fatigue deflection of OSB, Construction and Building Materials. 223 (2019) 1196–1203.

[10] T. Wang, Y. Yang, Y. Li, Z. Wang, Y. Gong, J. Zhou, M. Gong, Rolling shear failure damage evolution process of CLT based on AE technology and DIC method, European Journal of Wood and Wood Products. (2022).

[11] M. Diakhate, N. Angellier, R.M. Pitti, F. Dubois, On the crack tip propagation monitoring within wood material: Cluster analysis of acoustic emission data compared with numerical modelling, Construction and Building Materials. 156 (2017) 911–920.

[12] J. Oscarsson, A. Olsson, B. Enquist, Strain fields around knots in Norway spruce specimens exposed to tensile forces, Wood Science and Technology. 46 (2012) 593–610.

[13] H. Schreier, J.J. Orteu, M.A. Sutton, Image Correlation for Shape, Motion and Deformation Measurements, 2009.

[14] W. Li, J. Van den Bulcke, D. Mannes, E. Lehmann, I. De Windt, M. Dierick, J. Van Acker, Impact of internal structure on water–resistance of plywood studied using neutron radiography and X–ray tomography, Construction and Building Materials. 73 (2014) 171–179.

[15] B.Y. Choi, S.K. Himmi, T. Yoshimura, Quantitative observation of the foraging tunnels in Sitka spruce and Japanese cypress caused by the drywood termite Incisitermes minor (Hagen) by 2D and 3D X–ray computer tomography (CT), Holzforschung. 71 (2017) 535–542.

[16] J. Van den Bulcke, M.A. Boone, J. Dhaene, D. Van Loo, L. Van Hoorebeke, M.N. Boone, F. Wyffels, H. Beeckman, J. Van Acker, T. De Mil, Advanced X–ray CT scanning can boost tree–ring research for earth–system sciences, Annals of Botany. (2019).

[17] V. Biziks, J. Van Acker, H. Militz, J. Grinins, J. Van den Bulcke, Density and density profile changes in birch and spruce caused by thermo–hydro treatment measured by X–ray computed tomography, Wood Science and Technology. 53 (2019) 491–504.

[18] Wood–based panels. Oriented strand board (OSB). Definitions, classification and specifications, ISO International Standard. (2009).

[19] Y. Ying, R. Xin, W. Zeng, W. Liu, Fracture resistance curves of wood in the longitudinal direction using digital image correlation technique, Theoretical and Applied Fracture Mechanics. 114 (2021).

[20] Caliskan, U., Apalak, M. K., Low velocity bending impact behavior of foam core sandwich beams: Experimental, Composites Part B Engineering. 112 (2016) 158–175.

[21] S.K. Najafi, H. Sharifnia, M.A. Najafabadi, E. Landis, Acoustic emission characterization of failure mechanisms in oriented strand board using wavelet–based and unsupervised clustering methods, Wood Science and Technology. (2017) 1–14.